Journal of Digital Imaging (2023) 36:2278–2289
https://doi.org/10.1007/s10278-023-00853-6

An AI-Based Image Quality Control Framework for Knee Radiographs

Hongbiao Sun[1] · Wenwen Wang[1] · Fujin He[2] · Duanrui Wang[2] · Xiaoqing Liu[2] · Shaochun Xu[1] · Baolian Zhao[1] · Qingchu Li[1] · Xiang Wang[1] · Qinling Jiang[1] · Rong Zhang[1] · Shiyuan Liu[1] · Yi Xiao[1]

Received: 14 February 2023 / Revised: 14 May 2023 / Accepted: 17 May 2023 / Published online: 2 June 2023
© The Author(s) 2023

Abstract

Image quality control (QC) is crucial for the accurate diagnosis of knee diseases using radiographs. However, the manual QC process is subjective, labor intensive, and time-consuming. In this study, we aimed to develop an artificial intelligence (AI) model to automate the QC procedure typically performed by clinicians. We proposed an AI-based fully automatic QC model for knee radiographs using high-resolution net (HR-Net) to identify predefined key points in images. We then performed geometric calculations to transform the identified key points into three QC criteria, namely, anteroposterior (AP)/lateral (LAT) overlap ratios and LAT flexion angle. The proposed model was trained and validated using 2212 knee plain radiographs from 1208 patients and an additional 1572 knee radiographs from 753 patients collected from six external centers for further external validation. For the internal validation cohort, the proposed AI model and clinicians showed high intraclass consistency coefficients (ICCs) for AP/LAT fibular head overlap and LAT knee flexion angle of 0.952, 0.895, and 0.993, respectively. For the external validation cohort, the ICCs were also high, with values of 0.934, 0.856, and 0.991, respectively. There were no significant differences between the AI model and clinicians in any of the three QC criteria, and the AI model required significantly less measurement time than clinicians. The experimental results demonstrated that the AI model performed comparably to clinicians and required less time. Therefore, the proposed AI-based model has great potential as a convenient tool for clinical practice by automating the QC procedure for knee radiographs.

Keywords Artificial intelligence · Deep learning · Knee plain radiograph · Image quality control

Abbreviations

AI	Artificial Intelligence
AP	Anteroposterior
LAT	Lateral
ICCs	Intraclass consistency coefficients
CNNs	Convolutional neural networks
QC	Quality control
CI	Confidence intervals
SONK	Spontaneous osteonecrosis of the knee

Introduction

The knee joint is one of the largest and most complex joints in the human body and is subjected to strong gravitational forces [1]. Knee injuries can result from physical activities, aging, wear-and-tear, and various diseases, such as osteoarthritis (OA), rheumatic arthritis, spontaneous osteonecrosis of the knee (SONK), and knee instability [2–4]. Due to its frequency of injury, the knee joint is commonly examined in clinical practice. Anteroposterior (AP) and lateral (LAT) knee radiographs are currently the most commonly used imaging methods for assessing and diagnosing knee problems such as OA and SONK [4–8]. Kellgren and Lawrence [9] were pioneers in developing a classification system for osteoarthritis (OA) based on radiographs of the knee. They used AP knee radiographs and assigned a grade from 0 to 4 to each radiograph, with higher grades indicating increasing severity of OA. Subsequent research [10, 11] has shown that flexion radiographs (where the knee is flexed at 30 to 60°) can provide a more precise assessment of OA degeneration and narrowing,

Hongbiao Sun, Wenwen Wang and Fujin He contributed equally.

✉ Shiyuan Liu
radiology_cz@163.com

✉ Yi Xiao
cz-xiaoyi@smmu.edu.cn

[1] Department of Radiology, Shanghai Changzheng Hospital, Naval Medical University, No.415 Fengyang Road, Huangpu District, Shanghai 200003, China

[2] Deepwise Artificial Intelligence Laboratory, Beijing 100089, China

leading to more accurate diagnosis and treatment. Therefore, obtaining high-quality knee radiographs is crucial for the accurate diagnosis and treatment of knee diseases [6, 10, 11]. Clinicians' decision-making regarding disease diagnosis and treatment can be compromised by low-quality radiographs, which can directly impact patient care [12]. However, the rejection rate for clinically qualified knee radiographs is often between 8 and 12%, indicating the need for improvements [13, 14].

Quality control (QC) is crucial in ensuring sufficient image quality for accurately diagnosing knee diseases. Typically, QC of knee joint radiographs involves quantitative measurements of imaging quality, such as the signal-to-noise ratio, level of sharpness, and number of artifacts, along with a number of positioning criteria. These criteria include the overlap ratio of the fibular head with the tibia on AP and LAT projections, the flexion angle on LAT projections, sufficient overlap of the femoral condyles on LAT projections, femoral and tibial condyles symmetry on AP projections, patella position on both AP and LAT projections, and visualization of the joint space. To qualify as clinically acceptable, knee joint radiographs must meet specific criteria [15], as follows:

> For AP knee radiographs, the following must be met: (1) The image should show the femoral and tibial condyles as well as the fibular head, with the articular surface in the center of the image. (2) The capitellum of the fibula should only slightly overlap with the tibia. (3) All bone textures of the knee joint should be clearly visible, and the surrounding soft tissue should be visible. (4) The knee joint should be fully displayed in the center of the image and parallel to the long axis of the image.
>
> For LAT knee radiographs, the following criteria must be met: (1) The knee joint space should be in the center of the image, and the femoral condyle and tibial plateau should overlap well. (2) The patella should be displayed laterally, with a clear gap with the femur, and the articular surface border should be sharp and without shadowing. (3) There should be minimal overlap of the femur and tibial plateau. (4) All bone textures of the knee joint should be clearly visible, as should the surrounding soft tissues.

Today, QC of knee joint AP and LAT radiographs is mainly performed through manual evaluation, which can be subjective and influenced by factors such as radiologist experience, cognitive level, fatigue, and environmental conditions, among others; thus, it can be challenging to meet clinical requirements with this approach [6, 10]. Therefore, there is an urgent need for automated, real-time radiograph quality analysis to assist technicians in determining the need for re-examination before the patient leaves the X-ray room, saving time and improving patient satisfaction [16].

Recent advancements in artificial intelligence (AI), particularly in deep-learning-based techniques, have enabled the development of convolutional neural networks (CNNs) with immense potential in various medical imaging applications such as recognition, classification, segmentation, diagnosis, and even decision-making [17–23]. With access to large amounts of labeled data, certain AI models based on deep learning have been shown to perform comparably or even better than human experts in assisting clinicians with disease screening and identification, resulting in improved work efficiency. Additionally, these models play a significant role in clinical education by enhancing the skills of junior radiologists [24, 25]. Previous studies have demonstrated the effectiveness of CNNs in performing image QC of chest radiographs [26–28], where the AI-based QC model automatically measured three quality criteria of AP chest radiographs: correct inclusion of lungs at all four edges, patient rotation, and inspiration. These studies found that the AI model achieved good agreement with clinicians, suggesting that the AI model can automate chest radiograph QC.

In this study, we aimed to investigate the feasibility of automated QC for knee joint radiographs using AI. We identified the three most critical and error-prone criteria for knee joint radiograph positioning, including the overlap ratio of the fibular head with the tibia on AP and LAT projections, as well as the flexion angle on LAT projections. The objective was to compare the performance of our proposed AI-based model with observations made by clinicians to assess whether the AI-based QC model can automate the output of clinicians in knee radiograph QC.

Materials and Methods

Ethics Statement

This study was approved by the Institutional Review Board of Shanghai Changzheng Hospital (2022SL071) before patient information was accessed, and the requirement for informed patient consent was waived due to the retrospective nature of the analysis and the anonymity of the data.

Data Collection

We retrospectively collected 2,212 knee joint plain radiographs from 1208 patients from the Picture Archiving and Communication System (PACS) of Shanghai Changzheng Hospital (also referred to as Center 1) to train and validate the proposed AI model. Of these radiographs, 910 were AP radiographs, and 1302 were LAT radiographs. Specifically, 1638 plain radiographs from 796 patients (including 597 AP radiographs and 1041 LAT radiographs) were randomly selected as the training cohort, while the remaining 574 images from 412 patients (including 313 AP radiographs and 261 LAT radiographs) were used as the internal validation cohort. It is worth mentioning that we used a patient-wise partitioning strategy for the training and validation cohorts, ensuring that images from a single patient were only included in either the training or validation dataset, but not both.

To further validate the generalizability of the proposed AI-based QC model across different hospitals, an independent external validation cohort was collected from six other hospitals (referred to as Centers 2–7) that included 1572 knee radiographs from 753 patients, including 912 AP radiographs and 660 LAT radiographs, as shown in Fig. 1. In this study, we focused on performing QC for individual images rather than patient disease diagnosis, and so QC performance was evaluated at the individual-image level rather than at the patient level.

The data collected for this study adhered to the following inclusion and exclusion criteria. Radiographs were included if they (1) were taken from patients over 18 years old; (2) were plain knee joint radiographs; and (3) were obtained in accordance with standard guidelines [29]. Radiographs were excluded if (1) they were not AP or LAT projections of the knee joint; (2) they were blurred or occluded, thus affecting the observation of knee joint structures; (3) the knee joint depicted on the radiograph exhibited fractures, foreign bodies, postoperative changes, or severe osteoarthritis; or (4) they showed multiple knee joints in a single image.

All images were captured using equipment from Philips, General Electric or Canon, and any sensitive information was fully anonymized. Table 1 shows the data distribution for all cohorts.

Data Annotations

Plain knee radiographs are commonly used to diagnose knee joint diseases due to their ability to reveal the structural information of the knee. In this study, we selected three of the most critical and computationally challenging QC criteria for knee radiographs to evaluate the performance of an AI-based model against clinicians. These criteria are defined as follows:

1. Anteroposterior fibular head overlap ratio (AP overlap ratio): measures the overlap ratio between the fibular head and the tibia on AP knee plain radiographs.
2. Lateral fibular head overlap ratio (LAT overlap ratio): measures the overlap ratio between the fibular head and the tibia on LAT knee plain radiograph.
3. Flexion angle of the lateral knee (LAT flexion angle): measures the angle between the femur and the tibia on LAT knee plain radiograph.

To ensure the accuracy of the annotations, two associate chief musculoskeletal (MSK) radiologists with 10 and 13 years of experience first annotated all plain knee radiographs with key points. A committee of two chief MSK radiologists with 26 and 36 years of experience then reviewed all annotations and corrected any misplaced key points. Two other experts simultaneously reviewed all annotations, and any ambiguous labels were discarded. All annotations were then confirmed to be consistent and indisputable.

Preprocessing

All AP/LAT knee radiographs were converted from raw DICOM format to npy format using Python and SimpleITK [30]. To enhance the visualization of skeletal features and remove redundant information, we adjusted the displayed details using window width and window level as calculated by adaptive histogram equalization with limited contrast.

Computing of QC Criteria

Computing QC results for overlap ratios or flexion angle directly from images is challenging. To address this problem, we defined key points that describe the important positions of knee joints in an image. According to the QC requirements, for the AP knee plain radiographs, we used 5 key points, and for the LAT knee plain radiographs, we used 9 key points. Table 2 describes the definitions of these key points.

Figure 2 shows examples of predefined key points (A–I) and their corresponding auxiliary lines on AP and LAT knee plain radiographs. The line connecting key points A and B represents the diaphyseal orientation of the fibula, defined as L_1. The distance from key point C to line L_1 is defined as Sc, the distance from key point D to line L_1 is defined as Sd, and the distance from key point E to line L_1 is defined as Se. The overlap ratio is calculated using $(S_c - S_e)/(S_c - S_d)$, as shown in Fig. 2a, if key points E and C are located on the same side of straight line L1; otherwise, it is calculated using $(S_c - S_e)/(S_c - S_d)$, as shown in Fig. 2b. The line connecting key points F and G represents the diaphyseal orientation of the femur, defined as L_2. The line connecting key points H and I represents the diaphyseal orientation of the tibia, defined as L_3. The LAT flexion angle is defined as the angle between line L_2 and line L_3.

It is important to note that key points A, B, F, G, I, and H are used to determine the diaphyseal orientation of the tibia, femur, and fibula. However, these key points are not unique, and slight movement along the diaphyseal orientation will not affect the finalization of the diaphyseal orientation. For instance, key points A and B can be slightly adjusted along line L_1, but it is essential to ensure that the point is in the

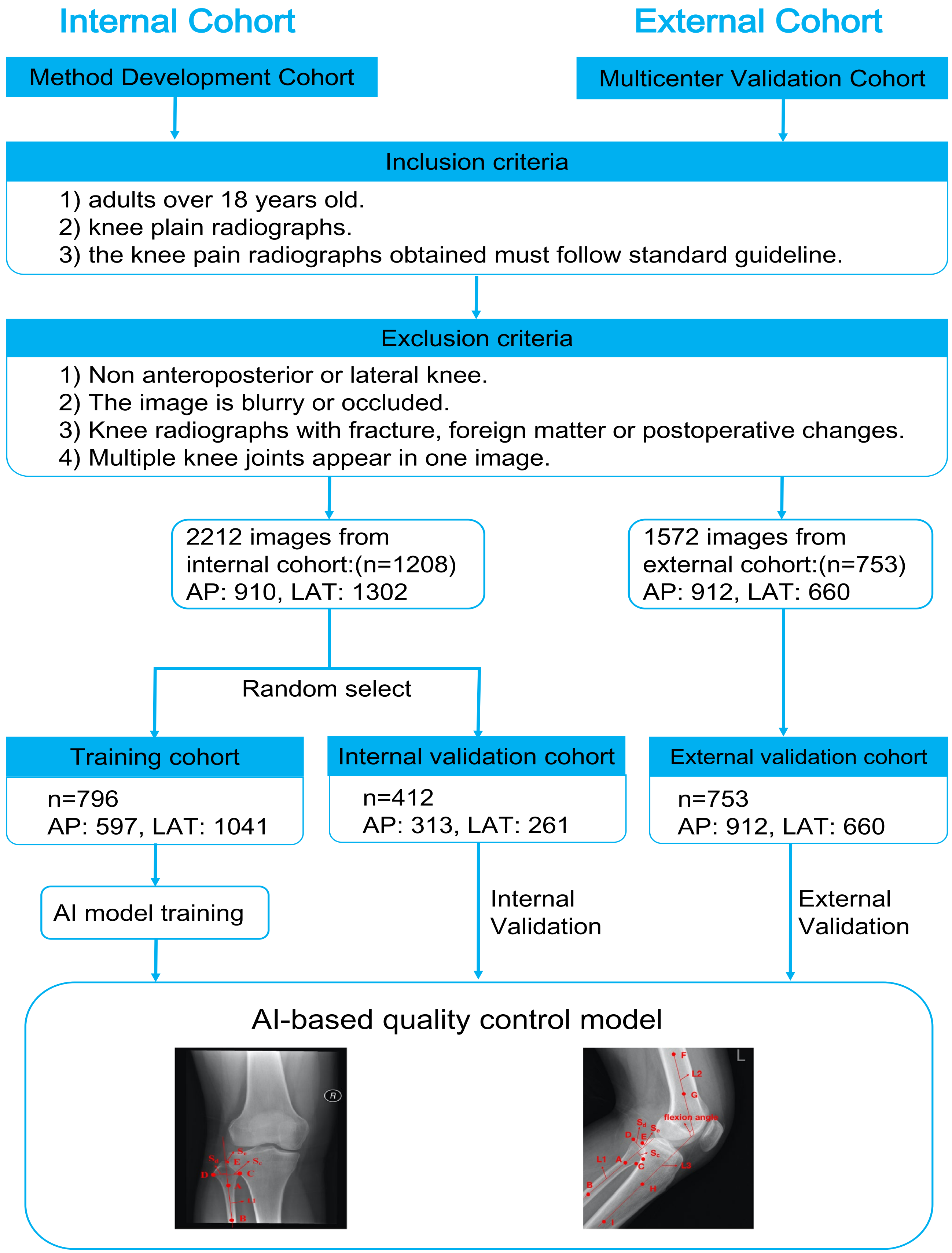
Internal Cohort
External Cohort
Method Development Cohort
Multicenter Validation Cohort
Inclusion criteria
1) adults over 18 years old.
2) knee plain radiographs.
3) the knee pain radiographs obtained must follow standard guideline.
Exclusion criteria
1) Non anteroposterior or lateral knee.
2) The image is blurry or occluded.
3) Knee radiographs with fracture, foreign matter or postoperative changes.
4) Multiple knee joints appear in one image.
2212 images from internal cohort:(n=1208) AP: 910, LAT: 1302
1572 images from external cohort:(n=753) AP: 912, LAT: 660
Random select
Training cohort
n=796
AP: 597, LAT: 1041
Internal validation cohort
n=412
AP: 313, LAT: 261
External validation cohort
n=753
AP: 912, LAT: 660
AI model training
Internal Validation
External Validation
AI-based quality control model
R
S_d
S_e
S_c
E
C
D
A
L1
B
L
F
L2
G
flexion angle
L3
H
I

◂**Fig. 1** Inclusion and exclusion criteria for this study. A total of 3784 knee plain radiographs were used to train and validate the generalization performance of the proposed AI-based QC model

middle of the backbone cross-section (in the vertical direction of L_1).

The Proposed AI-Based QC Model

In this study, we used an HR-Net-based framework [31] to design our automatic QC model for knee joint radiographs, as shown in Fig. 3. Our model was trained to detect a set of predefined key points, and auxiliary lines were drawn to aid in the interpretation of key measurements, as precise values for knee flexion angle and overlap ratios are not directly available. Finally, we used a set of simple but effective geometric calculations to compute the overlap ratio of the fibular head with the tibia on AP and LAT projections, as well as the flexion angle on LAT projections.

More specifically, we first applied an HR-Net [31] model pretrained using ImageNet [32] as a feature extraction backbone to detect predefined key points (key points A–E for AP knee radiographs and A–I for LAT knee radiographs). Auxiliary lines were then drawn to interpret key measurements such as the diaphyseal orientation of the tibia, femur, and fibular head and the overlap between the fibular head and the tibia. Subsequently, geometric calculations were performed to calculate the overlap ratio of the fibular head and the tibia and the angle between the femur and the tibia.

As shown in Fig. 3, HR-Net is a parallel multiresolution and multibranch network framework that ensures semantic information interaction between different branches and maintains high resolution throughout the whole process. Here, semantic information refers to the computed image features at different scales. The model starts from a stem block that decreases the input resolution to 1/4 by using two stride-2 3 × 3 convolutions; the resulting image then serves as the input of the multiresolution and multibranch network. A high-resolution subnetwork is then used as the first stage (S1 in Fig. 3), and the previous high resolution is maintained (1/4 of the original input resolution) throughout the whole process. At each new stage, a high-to-low resolution stream is added in parallel and connected to the multiresolution streams. The later stages not only consist of the resolutions from the previous stage but also have an extra lower resolution stream. Four stages are applied in the whole process, and the number of channels C is doubled while the resolution gradually drops to half (i.e., C = 32, 64, 128, and 256 for feature maps F1, F2, F3, and F4, respectively).

To make better use of multiresolution information, an exchange model is used to exchange information across parallel subnetworks and is repeated several times (e.g., every 4 residual units; only 2 residual units are shown in Fig. 1). In the exchange model, information from different subnetworks is downsampled/upsampled to the same resolution, and 3 × 3 convolutions with stride 1 are used to maintain channel consistency. For example, if the feature $I_r, r = 1, 2, 3$ in stage 3 (S3) is associated with the output feature $O_r, r = 1, 2, 3$ after an exchange model, and the final output is the sum of the three inputs $o_r = \int_1^r(I_1) + \int_2^r(I_2) + \int_3^r(I_3)$, where r is the resolution index, an extra output $o_r = \int_1^4(I_1) + \int_2^4(I_2) + \int_3^4(I_3)$ is obtained across stages (from S3 to S4). The model repeats the information exchange across the multiresolution subnetworks, with S2, S3, and S4 containing 1, 4, and 3 exchange models, respectively. This enables more effective multiscale fusion learning and allows subnetworks with different resolutions to contribute different pieces semantic information, leading to a more expressive final feature map. Subsequently, features F2-F4 are converted to be consistent with feature F1 using upsampling and 1*1 Conv (H*W*C, F1 is only 1*1 Conv), and then features F1-F4 are concatenated as O1. Finally, a 1 * 1 conv is used to obtain the final output with shape H*W*9. Afterward, the location with the highest probability (maximum activation) in the output probability map is considered the detected key point.

Table 1 Data distribution for different cohorts

	No. of patients	No. of APs	No. of LATs
Training cohort (Center 1)	796	597	1041
Internal validation cohort (Center 1)	412	313	261
External validation cohort	753	912	660
Center 2	20	20	16
Center 3	144	279	215
Center 4	168	174	111
Center 5	244	266	209
Center 6	83	81	51
Center 7	94	92	58

Table 2 Detailed description of key points

AP/LAT	Key point	Description
AP/LAT	A/B	Diaphyseal orientation of the fibula is determined by two points on the center of the fibula diaphysis: key point A in the mid-fibula and key point B in the distal fibula
	C	The key point on the head of the fibula closest to the tibia
	D	The key point on the fibular head furthest away from the tibia
	E	The key point where the fibular head overlaps the tibia
LAT	F/G	Diaphyseal orientation of the femur is determined by two points on the center of the femur diaphysis: key point F in the proximal femur and key point G in the mid-femur
	H/I	Diaphyseal orientation of the tibia is determined by two points on the center of the tibia diaphysis: key point H in the proximal tibia and key point I in the mid-tibia

Implementation Details

In this study, we used the mean square error (MSE) loss to measure the deviation between the regressed heatmaps and the ground-truth heatmaps, which were generated using a 2D Gaussian distribution with sigma = 2. It should be recalled that the LAT knee joint radiograph has four additional key points over the AP knee joint. To manage this difference, we set the regression objective to 0 for these four key points on the AP knee radiographs. This approach offers two benefits: the model can handle both AP/LAT knee radiographs, and the input image can be automatically identified as an AP or LAT knee radiograph based on the number of detected key points.

We trained the model using stochastic gradient descent (SGD) with an initial learning rate of 0.002, which decayed by 10 after 50 epochs and 56 epochs. The momentum was set to 0.9, and the weight decay was set to 0.0001. We used a mini-batch size of 4 and trained the model for a total of 60 epochs. The short side of the input image was resized to 288 while keeping the original aspect ratio. To increase the diversity of the data, data augmentation strategies including random flips and random inversions with a probability of 0.5 were used.

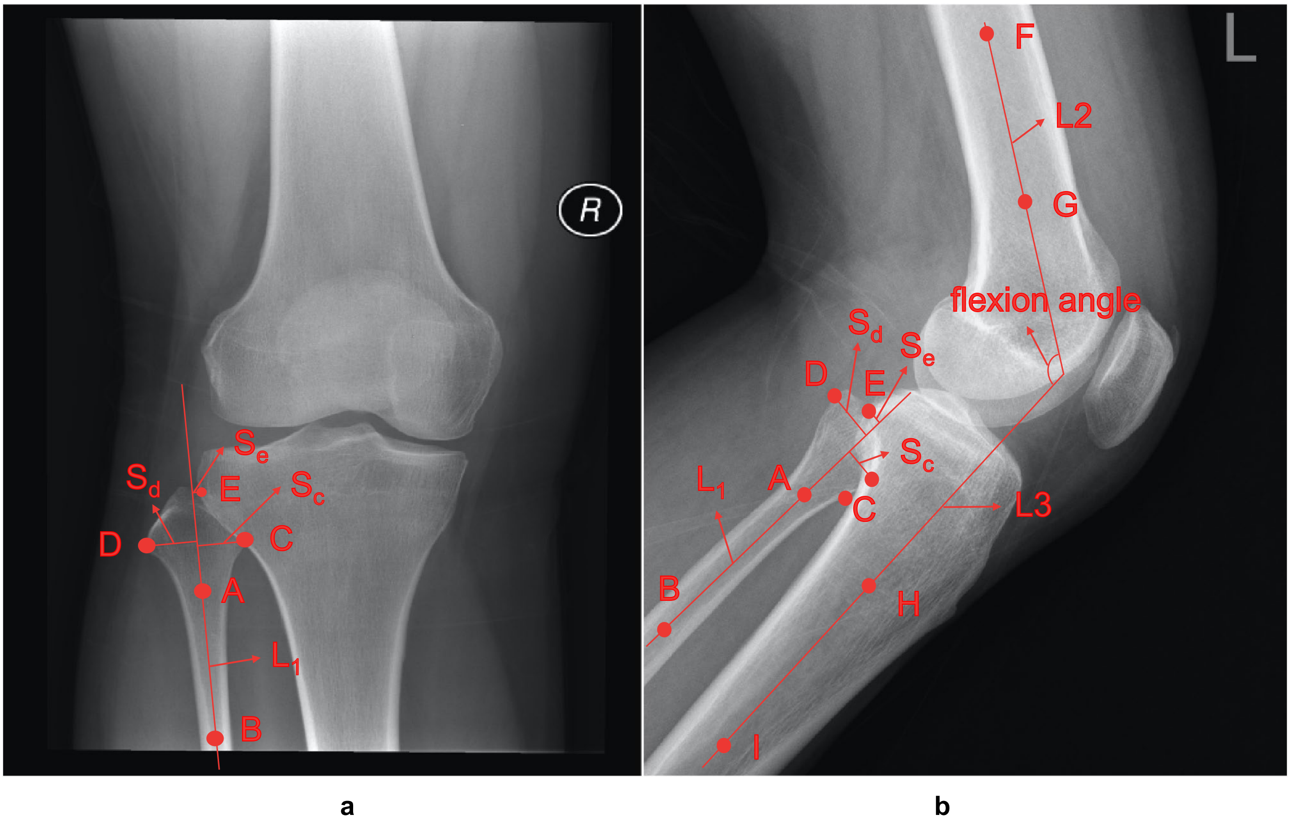

Fig. 2 Example annotations of predefined key points and their corresponding auxiliary lines. **a** AP knee plain radiograph. **b** LAT knee plain radiograph. Auxiliary lines L1, L2, L3, vertical lines Sc, Sd, Se and flexion angle are all shown

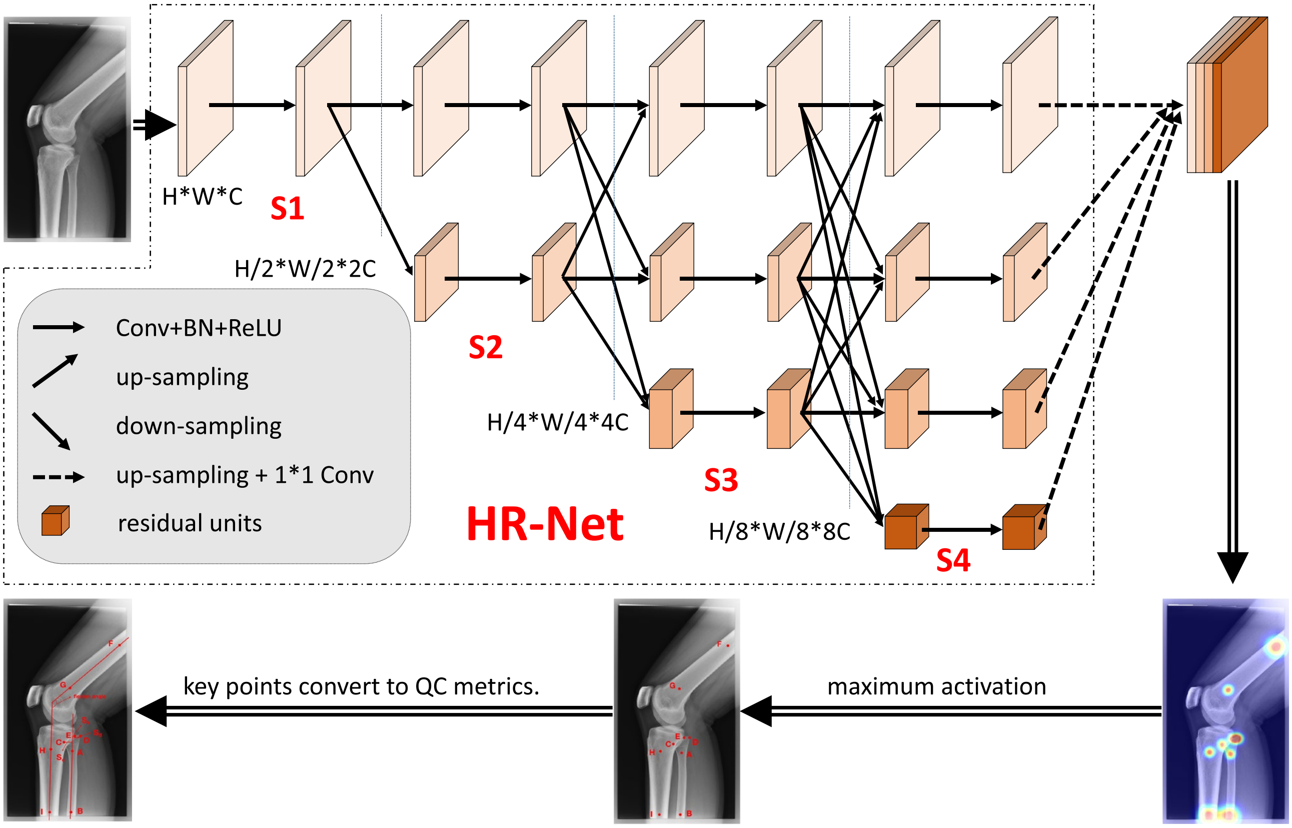

Fig. 3 Pipeline of the proposed AI-based QC model

Experiments were implemented using the open-source toolbox mmdetection and pytorch [33]. To speed up training, we used four NVIDIA 1080TI GPUs to train our model.

Results

Primary Validation

We evaluated the performance of the proposed AI-based QC model by measuring its agreement with clinicians using the intraclass correlation coefficient (ICC) [34]. We chose two-way random effects, absolute agreement, and a single rater as our measurement model, abbreviated as ICC(2,1) [34]. ICC > 0.75 indicates good reliability, and ICC > 0.9 indicates excellent reliability. *p* values less than 0.05 were considered to indicate statistical significance using independent-samples t tests.

As shown in Table 3, the ICCs of the proposed AI-based QC model and clinicians in the internal validation cohort were 0.952 (95% confidence intervals (CI): 0.94–0.96), 0.895 (95% CI: 0.87–0.91), and 0.993 (95% CI: 0.99–0.99) for the AP overlap ratio, LAT overlap ratio, and LAT

Table 3 ICC measurements between clinicians and the AI-based model in terms of AP overlap ratio, LAT overlap ratio, and LAT flexion angle

Data Sources	AP overlap ratio (95% CI)	LAT overlap ratio (95% CI)	LAT flexion angle (95% CI)
Internal validation cohort			
Center 1	0.952 (0.94–0.96)	0.895 (0.87–0.91)	0.993 (0.99–0.99)
External validation cohort			
Center 2	0.913 (0.79–0.96)	0.909 (0.66–0.97)	0.984 (0.87–1.0)
Center 3	0.915 (0.86–0.94)	0.874 (0.83–0.91)	0.976 (0.97–0.98)
Center 4	0.930 (0.91–0.95)	0.869 (0.81–0.91)	0.978 (0.91–0.99)
Center 5	0.940 (0.92–0.95)	0.827 (0.78–0.87)	0.997 (0.99–1.0)
Center 6	0.934 (0.90–0.96)	0.877 (0.80–0.93)	0.993 (0.99–1.0)
Center 7	0.911 (0.87–0.94)	0.825 (0.72–0.89)	0.983 (0.95–0.99)
Mean	0.934 (0.92–0.94)	0.856 (0.83–0.88)	0.991 (0.99–0.99)

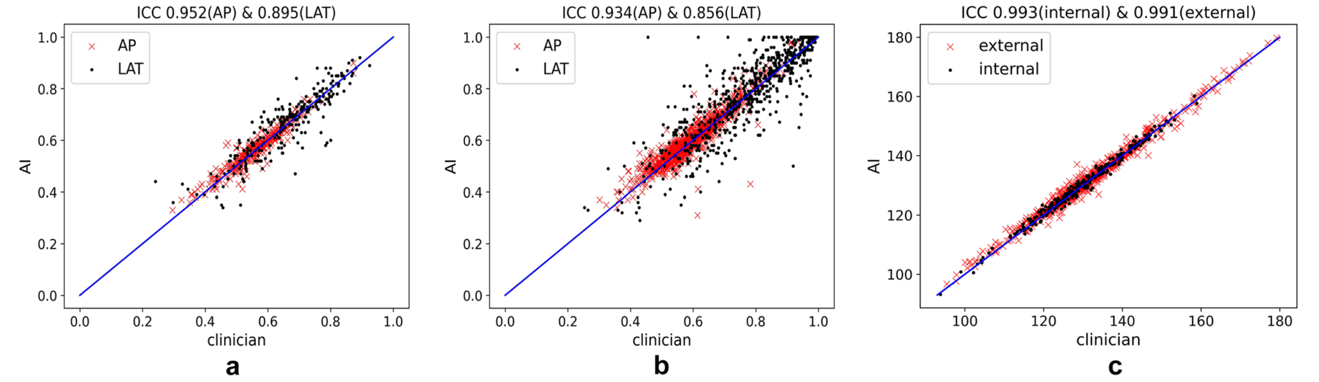

Fig. 4 Scatter plots of the correlations between the AI model and clinicians. **a** AP/LAT overlap ratios in the internal validation cohort, **b** AP/LAT overlap ratios in the external validation cohort, **c** LAT flexion angles in both the internal and external validation cohorts

flexion angle, respectively. There were no statistically significant differences between clinicians and the AI-based model on any of the three criteria, namely, AP overlap ratio ($p = 0.498$), LAT overlap ratio ($p = 0.858$), and LAT flexion angle ($p = 0.777$). For the external validation cohort, the mean ICCs between clinicians and the AI-based model were 0.934 (95% CI: 0.92–0.94), 0.856 (95% CI: 0.83–0.88), and 0.991 (95% CI: 0.99–0.99) for the AP overlap ratio, LAT overlap ratio, and LAT flexion angle, respectively. Similarly, there were no statistically significant differences between clinicians and the AI-based model in terms of AP overlap ratio ($p = 0.093$), LAT overlap ratio ($p = 0.278$), and LAT flexion angle ($p = 0.632$). These results demonstrate that the QC performance of the proposed AI model is comparable to that of clinicians when testing on data within and across different centers, indicating great potential for application in clinical practice.

Figure 4 illustrates the correlation between the AI-based model and clinicians in terms of AP/LAT overlap ratios and LAT flexion angle. Specifically, Fig. 4a, b depicts the scatter points for the AP/LAT overlap ratios in the internal and external validation cohorts, respectively, while Fig. 4c shows the scatter points for the LAT flexion angle in both cohorts. The blue line in the center of each plot indicates exact agreement between the AI model and clinicians, meaning no deviation between the two.

In general, the scatter points for the AP/LAT overlap ratios in Fig. 4a, b were closer to the centerline on the AP knee radiographs, suggesting a slight deviation. However, on the LAT knee radiographs, the scatter points were more spread out relative to the centerline. This pattern was consistent across both internal and external validation cohorts. On the other hand, Fig. 4c shows high agreement between clinicians and the AI-based model for LAT flexion angle, with little deviation in either cohort.

To further quantify the agreement between the AI-based model and clinicians, Table 4 presents the mean, standard deviation, and maximum deviation of the AP/LAT overlap ratios in the internal and external validation cohorts. Notably, the mean, standard deviation, and maximum deviation of the LAT overlap ratio were consistently larger than those of the AP overlap ratio in both cohorts, which aligns with the scatter plots in Fig. 4. Since the LAT flexion angle ranges from 0 to 180, normalized values were also included in

Table 4 Means and standard deviations of absolute deviations between clinicians and the AI-based model in both the internal and external validation cohorts

	AP overlap ratio	LAT overlap ratio	LAT flexion angle*
Internal validation cohort			
Mean	0.019	0.040	1.049(0.006)
Standard deviation	0.018	0.039	0.748(0.004)
Max deviation	0.117	0.217	3.730(0.021)
External validation cohort			
Mean	0.024	0.058	1.289(0.007)
Standard deviation	0.026	0.058	1.109(0.006)
Max deviation	0.352	0.544	8.582(0.477)
p value	< 0.01	< 0.01	< 0.01

*The AP/LAT overlap ratio ranges between 0 and 1, while the LAT flexion angle ranges between 0 and 180; the numbers in parentheses represent normalized angles, ranging between 0 and 1. The *p* value was calculated based on the mean using t tests

Table 4 for a fair comparison. The normalized values demonstrate significant agreement between clinicians and the AI-based model in terms of LAT flexion angle, with more agreement observed in the internal validation cohort, which is also consistent with the findings shown in Fig. 4.

Comprehensive Performance Analysis

Our primary validation results showed that the proposed AI-based QC model performed poorer on LAT radiographs than on AP radiographs. Through a comprehensive visual analysis of knee plain radiographs, we found that occlusions were relatively common on the LAT knee joint radiographs, as shown in Fig. 5a, b, making identifying key point C difficult and resulting in inaccurate LAT overlap ratios. Additionally, the fibular head is prone to variations, such as the distortions shown in Fig. 5c, d, resulting in deviations in the final measurement results. Due to occlusion and variation, the fibular head overlap ratio is generally less consistent on LAT knee radiographs than on AP knee radiographs. In summary, the deviations on AP knee radiographs are generally lower than those on LAT knee radiographs, mainly due to the relatively better clarity and visibility of the knees on the AP projections.

Performance in Key Point Detection

Since HR-Net-based key point detection is the basis of the proposed AI-based QC model, we reported the quantitative performance of the key point detection model in terms of average precision (AP) and average recall (AR) [35]. Object key point similarity (OKS) was used to measure the deviation in the key points, calculated as $OKS = \frac{\sum_i \exp(-d_i^2/2s^2k_i^2\delta(v_i>0))}{\sum_i \delta(v_i>0)}$. Here, $s2$ is the object scale, which we set as the area of the smallest bounding box containing all key points; di is the Euclidean distance between a detected key point and its corresponding ground truth; vi is the visibility flag; and ki is a predefined constant derived from the statistics of annotation deviations. Generally, $\mathrm{k_i} = 2\sigma_\mathrm{i}$, where σ_i is the standard deviation, which differs for different key points. We applied the mean of the statistical results of the key point detection statistics [35]; that is, σ_i for key points A–I were [0.083, 0.083, 0.029, 0.029, 0.029, 0.083, 0.083, 0.083, 0.083].

As shown in Table 5, our experimental results showed that our key point detection model achieved excellent mean average precision (mAP) values. Figure 6 also visualizes examples of key point detection results, where red key points and lines are clinician annotations, and blue key points and lines represent the AI model's generated results. As expected, we observed that occlusion and ambiguity affected the identification of key point C, which could lead to inaccurate measurement results.

Discussion

In this study, we proposed an AI-based fully automatic QC model for knee radiographs. The model uses HR-Net to identify predefined key points in images and then performs a set of geometric calculations to transform these key points into three QC criteria: the AP overlap ratio, LAT overlap ratio, and LAT flexion angle. The proposed model was trained and validated using a total of 2212 knee plain radiographs, including 910 AP radiographs and 1,302 LAT radiographs. An additional 1572 knee radiographs, including 912 AP radiographs and 660 LAT radiographs, were also collected from six external centers as an external validation cohort.

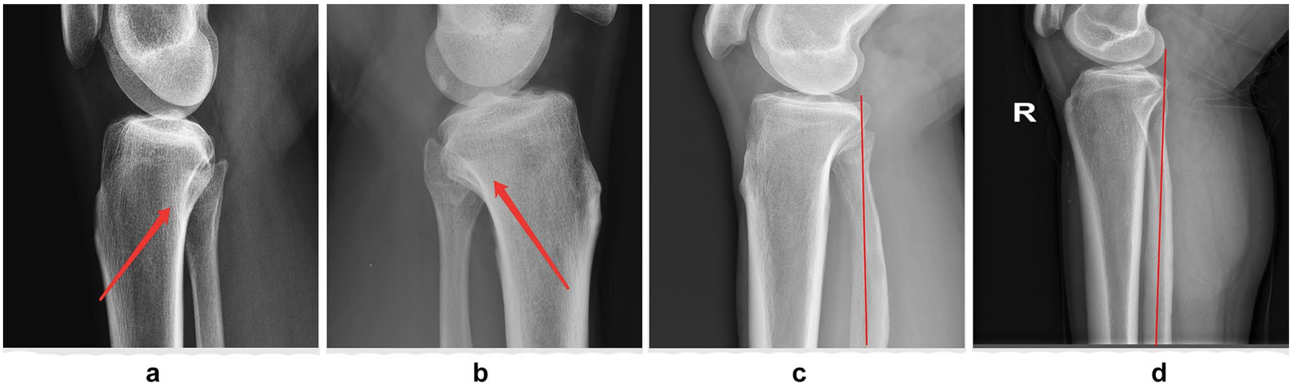

Fig. 5 Visualization of occlusion and variation of the fibular head. **a** and **b** show occlusion of the fibular head, making the location of key point C ambiguous and resulting in inaccurate LAT overlap ratios. In **c** and **d**, the fibular head is bent due to variations, where the red line indicates the orientation of the fibula. The curved fibular head distorts the calculations of Sc, Sd, and Se, resulting in inaccurate LAT overlap ratios. Due to occlusion and variation, the fibular head overlap ratio is generally less consistent on LAT knee radiographs than on AP knee radiographs

Table 5 Performance in key point detection

		mAP*	AP50	AP75	mAR*	*p* value
AP	Internal validation cohort	0.988	0.989	0.989	0.996	< 0.01
	External validation cohort	0.922	0.986	0.986	0.955	
LAT	Internal validation cohort	0.846	0.990	0.972	0.903	< 0.01
	External validation cohort	0.788	0.990	0.922	0.852	

*mAP is the mean average precision, mAR is the mean average recall, and the *p* value is calculated based on the mAP using *t* tests

Our results demonstrated that the proposed AI-based model achieved similar reliability to that of clinicians on all three QC criteria. In the internal validation cohort, the ICCs for the overlap ratios of the AP fibular head and LAT fibular head and the LAT flexion angle were 0.952, 0.895, and 0.993, respectively, while the corresponding ICCs for the external validation cohort were 0.934, 0.856, and 0.991. Our experimental results demonstrated that the differences in the performances between clinicians and the AI-based model on all three QC criteria in the internal and external validation cohorts were not significant. The proposed model was substantially more efficient, taking an average of 0.52 ± 0.10 (AP)/0.52 ± 0.10 (LAT) seconds to process a knee plain radiograph versus the 15.23 ± 1.33 (AP)/24.49 ± 1.91 (LAT) seconds required by clinicians. Therefore, the proposed AI-based QC model has great potential as an effective and efficient auxiliary tool to help clinicians reduce the time and effort in performing QC while maintaining objective, consistency, and comparable accuracy.

However, this study also had several limitations. First, we found statistically significant differences between the internal and external validation cohorts on all three QC criteria and our key point detection in our experimental results. This outcome was expected, given that the training and internal

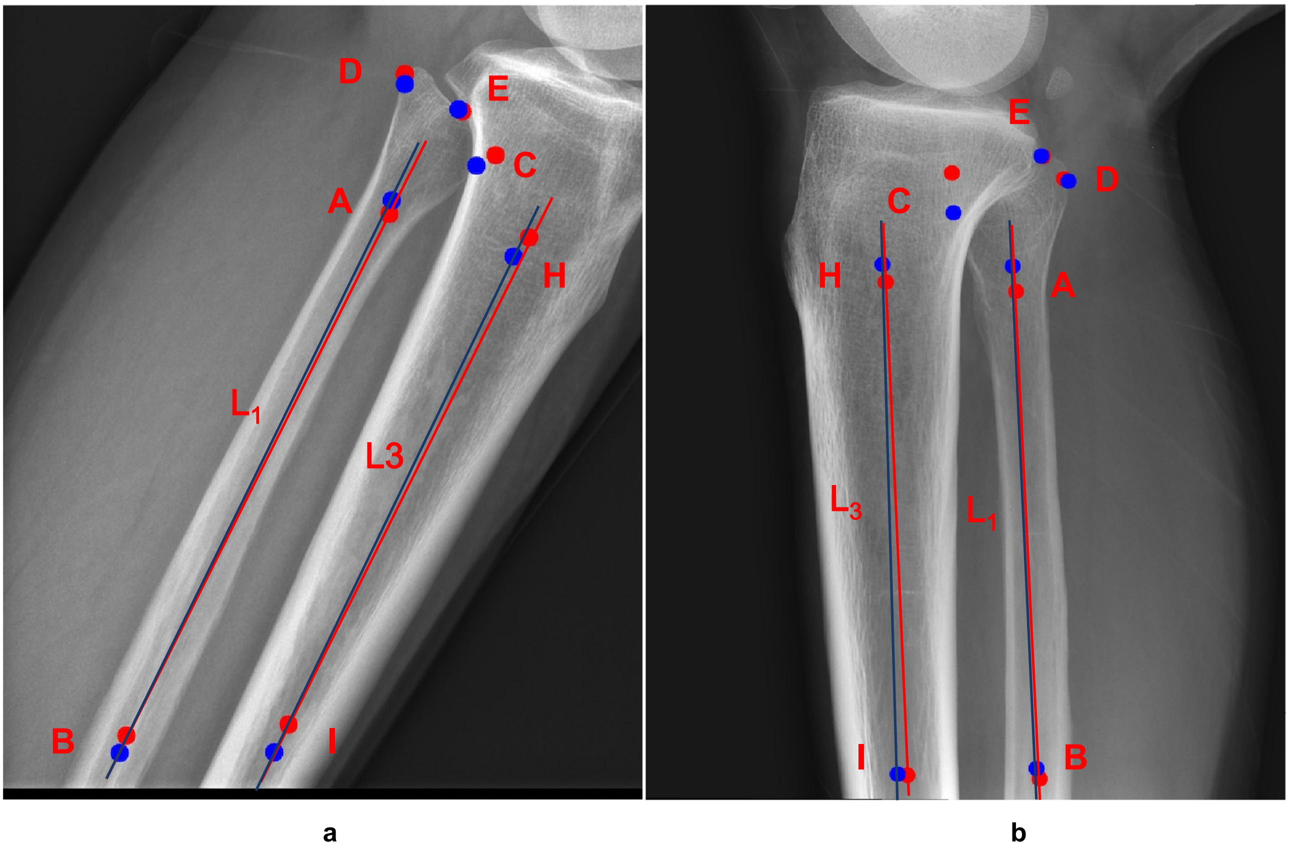

Fig. 6 Visualization of key point detection, where the red key points and lines are from the clinician's annotations and the blue key points and lines were generated by the AI model. Both occlusion and blurring affected the identification of key point C

validation cohorts were obtained from the same center, whereas the external validation cohort was sourced from six other centers. Increasing the diversity of data sources in the training cohort could address this issue. Second, the performance in key point detection needs to be improved, especially on LAT knees, due to factors such as occlusion, blur, and variation that can affect the detection of key points. Additionally, key points A, B, F, G, H, and I, located along the diaphyseal orientation, are not well defined, and annotations may vary between clinicians. Further exploration of other methods of determining the diaphyseal orientation is necessary. As a feasibility study, we only investigated three QC criteria for image positioning, and more quantitative measures, including imaging quality and other positioning criteria, will be explored in the future for a more complete, clinically applicable QC system. Finally, other quantitative metrics will also be explored to measure agreement between clinicians and the AI-based model.

In conclusion, the proposed AI-based QC model, by incorporating three objective QC criteria, including the AP overlap ratio, LAT overlap ratio, and LAT flexion angle, achieved reliability comparable to that of clinicians. In clinical practice, clinicians are often too busy to carefully measure knee radiographs. The proposed AI-based QC model can automate the QC of knee radiographs with a performance that is highly consistent with traditional manual evaluation but more efficient. Therefore, the proposed AI-based model has great potential for automating the QC of knee radiographs by clinicians while offering great conveniences to clinical practice.

Author Contribution Hongbiao Sun: Conceptualization; methodology; formal analysis; resources; writing, original draft; investigation; project administration; funding acquisition. Wenwen Wang: Conceptualization, methodology, formal analysis, resources, supervision, validation, investigation, project administration. Fujin He: Conceptualization; methodology; formal analysis; resources; writing, original draft; project administration; visualization; software; data curation; investigation. Duanrui Wang: Formal analysis; data curation; resources; writing, review and editing; validation. Xiaoqing Liu: Conceptualization; methodology; formal analysis; writing, review and editing; supervision; validation; project administration. Shaochun Xu: Investigation, formal analysis, resources, data curation. Baolian Zhao: Investigation, formal analysis, resources, data curation. Qingchu Li: Investigation, formal analysis, resources, data curation. Xiang Wang: Investigation, formal analysis, resources, data curation. Qinling Jiang: Investigation, formal analysis, resources, data curation. Rong Zhang: Investigation, formal analysis, resources, data curation. Shiyuan Liu: Conceptualization; methodology; formal analysis; writing, review and editing; supervision; project administration. Yi Xiao: Conceptualization; methodology; formal analysis; writing, review and editing; supervision; project administration; funding acquisition.

Funding This work was supported in part by the National Natural Science Foundation of China [No. 82271994]; the Special Military Medical Project of Shanghai Changzheng Hospital [No. 2019CZJS106]; the Contract grant sponsor: Pyramid Talent Project of Shanghai Changzheng Hospital; the Shenkang capacity enhancement project [NO. SHDC22022310-B]; the Military Commission surface project [NO. 22BJZ07]; the National Key Research and Development Program [No. 2022YFC2410000) and the National Health Commission Radiological Imaging Database Construction Project [NO. YXFSC2022JJSJ010].

Data Availability The data that support the findings of this study are available on request from the corresponding author. The data are not publicly available due to privacy or ethical restrictions.

Declarations

Ethics Approval and Consent to Participate This study was approved by the Institutional Review Board of Shanghai Changzheng Hospital (2022SL071) before patient information was accessed, and the requirement for informed consent of patients was waived due to the retrospective nature of the analysis and the anonymity of the data.

Competing Interests The authors declare no competing interests.

Open Access This article is licensed under a Creative Commons Attribution 4.0 International License, which permits use, sharing, adaptation, distribution and reproduction in any medium or format, as long as you give appropriate credit to the original author(s) and the source, provide a link to the Creative Commons licence, and indicate if changes were made. The images or other third party material in this article are included in the article's Creative Commons licence, unless indicated otherwise in a credit line to the material. If material is not included in the article's Creative Commons licence and your intended use is not permitted by statutory regulation or exceeds the permitted use, you will need to obtain permission directly from the copyright holder. To view a copy of this licence, visit http://creativecommons.org/licenses/by/4.0/.

References

1. Zlotnicki JP, Naendrup J-H, Ferrer GA, Debski RE. Basic biomechanic principles of knee instability. Current reviews in musculoskeletal medicine. 2016;9(2):114-122.
2. Gage BE, McIlvain NM, Collins CL, Fields SK, Comstock RD. Epidemiology of 6.6 Million Knee Injuries Presenting to United States Emergency Departments From 1999 Through 2008. Acad Emerg Med. 2012;19(4):378–385.
3. Kong AP, Robbins RM, Stensby JD, Wissman RD. The Lateral Knee Radiograph: A Detailed Review. Journal of Knee Surgery. 2022;35(05):482-490.
4. Wang SM, Xiao ZB, Lu YF, Zhang ZW, Lv FJ. Radiographic optimization of the lateral position of the knee joint aided by CT images and the maximum intensity projection technique. Journal of Orthopaedic Surgery and Research. 2021;16(1).
5. Fu X, Wang W. Radiologic imaging techniques in diagnosis of patella alta. Chinese Journal of Tissue Engineering Research. 2012;16(39):7338-7344.
6. Mazzuca SA, Brandt KD, Katz BP. Is conventional radiography suitable for evaluation of a disease-modifying drug in patients with knee osteoarthritis? Osteoarthritis and Cartilage. 1997;5(4):217-226.
7. Akamatsu Y, Kobayashi H, Kusayama Y, Aratake M, Kumagai K, Saito T. Predictive factors for the progression of spontaneous osteonecrosis of the knee. Knee Surgery Sports Traumatology Arthroscopy. 2017;25(2):477-484.

8. Kohn MD, Sassoon AA, Fernando ND. Classifications in Brief: Kellgren-Lawrence Classification of Osteoarthritis. Clinical Orthopaedics and Related Research. 2016;474(8):1886-1893.
9. Kellgren JH, Lawrence JS. Radiological assessment of osteoarthrosis. Annals of the rheumatic diseases. 1957;16(4):494-502.
10. Rosenberg TD, Paulos LE, Parker RD, Coward DB, Scott SM. The 45-degree posteroanterior flexion weight-bearing radiograph of the knee. Journal of Bone and Joint Surgery-American Volume. 1988;70A(10):1479-1483.
11. Mason RB, Horne JG. The posteroanterior 45 degrees flexion weight-bearing radiograph of the knee. Journal of Arthroplasty. 1995;10(6):790-792.
12. Saleem M, Farid MS, Saleem S, Khan MH. X-ray image analysis for automated knee osteoarthritis detection. Signal Image and Video Processing. 2020;14(6):1079-1087.
13. Brealey S, Scally A, Hahn S, Thomas N, Godfrey C, Coomarasamy A. Accuracy of radiographer plain radiograph reporting in clinical practice: a meta-analysis. Clinical Radiology. 2005;60(2):232-241.
14. Jones AK, Polman R, Willis CE, Shepard SJ. One Year's Results from a Server-Based System for Performing Reject Analysis and Exposure Analysis in Computed Radiography. Journal of Digital Imaging. 2011;24(2):243-255.
15. Wang X, Chang D, Zhao C, Shan Q, Xu Z. Improvement of adult knee joint anteroposterior and lateral projection technique. Chinese medical journal. 2022;57(4):4.
16. Mushtaq J, Pennella R, Lavalle S, Colarieti A, Steidler S, Martinenghi CMA, et al. Initial chest radiographs and artificial intelligence (AI) predict clinical outcomes in COVID-19 patients: analysis of 697 Italian patients. European Radiology. 2021;31(3):1770-1779.
17. Havaei M, Davy A, Warde-Farley D, Biard A, Courville A, Bengio Y, et al. Brain tumor segmentation with Deep Neural Networks. Medical Image Analysis. 2017;35:18-31.
18. Ronneberger O, Fischer P, Brox T, editors. U-Net: Convolutional Networks for Biomedical Image Segmentation. 18th International Conference on Medical Image Computing and Computer-Assisted Intervention (MICCAI); 2015 Oct 05–09; Munich, GERMANY2015.
19. Yamashita R, Nishio M, Do RKG, Togashi K. Convolutional neural networks: an overview and application in radiology. Insights into Imaging. 2018;9(4):611-629.
20. Zhang SC, Sun J, Liu CB, Fang JH, Xie HT, Ning B. Clinical application of artificial intelligence-assisted diagnosis using anteroposterior pelvic radiographs in children with developmental dysplasia of the hip. Bone & Joint Journal. 2020;102B(11):1574-1581.
21. Tajbakhsh N, Suzuki K. Comparing two classes of end-to-end machine-learning models in lung nodule detection and classification: MTANNs vs. CNNs. Pattern Recognition. 2017;63:476-486.
22. Rodriguez-Ruiz A, Krupinski E, Mordang JJ, Schilling K, Heywang-Kobrunner SH, Sechopoulos J, et al. Detection of Breast Cancer with Mammography: Effect of an Artificial Intelligence Support System. Radiology. 2019;290(2):305-314.
23. Goldenberg SL, Nir G, Salcudean SE. A new era: artificial intelligence and machine learning in prostate cancer. Nature Reviews Urology. 2019;16(7):391-403.
24. He KM, Zhang XY, Ren SQ, Sun J, Ieee, editors. Delving Deep into Rectifiers: Surpassing Human-Level Performance on ImageNet Classification. IEEE International Conference on Computer Vision; 2015 Dec 11–18; Santiago, CHILE2015.
25. Buda M, Wildman-Tobriner B, Hoang JK, Thayer D, Tessler FN, Middleton WD, et al. Management Thyroid Nodules Seen on US Images: Deep Learning May Match Performance of Radiologists. Radiology. 2019;292(3):695-701.
26. Nousiainen K, Makela T, Piilonen A, Peltonen JI. Automating chest radiograph imaging quality control. Physica Medica-European Journal of Medical Physics. 2021;83:138-145.
27. Poggenborg J, Yaroshenko A, Wieberneit N, Harder T, Gossmann A. Impact of AI-based Real Time Image Quality Feedback for Chest Radiographs in the Clinical Routine. Cold Spring Harbor Laboratory Press. 2021.
28. Santosh KC, Candemir S, Jaeger S, Karargyris A, Antani S, Thoma GR. Automatically Detecting Rotation in Chest Radiographs Using Principal Rib-Orientation Measure for Quality Control. International Journal of Pattern Recognition and Artificial Intelligence. 2015;29(2).
29. Association ITBoCM, Association RBoCM. Expert consensus on breast imaging. Chinese Journal of Radiology. 2016(7):12.
30. Lowekamp BC, Chen DT, Ibanez L, Blezek D. The Design of SimpleITK. Frontiers in Neuroinformatics. 2013;7.
31. Sun K, Xiao B, Liu D, Wang JD, Soc IC, editors. Deep High-Resolution Representation Learning for Human Pose Estimation. 32nd IEEE/CVF Conference on Computer Vision and Pattern Recognition (CVPR); 2019 Jun 16–20; Long Beach, CA2019.
32. Deng J, Dong W, Socher R, Li LJ, Li K, Li FF, et al., editors. ImageNet: A Large-Scale Hierarchical Image Database. IEEE-Computer-Society Conference on Computer Vision and Pattern Recognition Workshops; 2009 Jun 20–25; Miami Beach, FL2009.
33. Paszke A, Gross S, Massa F, Lerer A, Bradbury J, Chanan G, et al., editors. PyTorch: An Imperative Style, High-Performance Deep Learning Library. 33rd Conference on Neural Information Processing Systems (NeurIPS); 2019 Dec 08–14; Vancouver, CANADA2019.
34. Koo TK, Li MY. A Guideline of Selecting and Reporting Intraclass Correlation Coefficients for Reliability Research. J Chiropr Med. 2016;15(2):155-163.
35. Common Objects in Context. https://cocodataset.org/#keypoints-eval. Accessed. 27 April 2023.

Publisher's Note Springer Nature remains neutral with regard to jurisdictional claims in published maps and institutional affiliations.